

First-principles study on oxidation effects in uranium oxides and high-pressure high-temperature behavior of point defects in uranium dioxide

Hua Y. Geng, Hong X. Song, K. Jin, S. K. Xiang, and Q. Wu

National Key Laboratory of Shock Wave and Detonation Physics, Institute of Fluid Physics, CAEP, P.O.Box 919-102 Mianyang, Sichuan 621900, People's Republic of China

Formation Gibbs free energy of point defects and oxygen clusters in uranium dioxide at high-pressure high-temperature conditions are calculated from first principles, using the LSDA+ U approach for the electronic structure and the Debye model for the lattice vibrations. The phonon contribution on Frenkel pairs is found to be notable, whereas it is negligible for the Schottky defect. Hydrostatic compression changes the formation energies drastically, making defect concentrations depend more sensitively on pressure. Calculations show that, if no oxygen clusters are considered, uranium vacancy becomes predominant in overstoichiometric UO_2 with the aid of the contribution from lattice vibrations, while compression favors oxygen defects and suppresses uranium vacancy greatly. At ambient pressure, however, the experimental observation of predominant oxygen defects in this regime can be reproduced only in a form of cuboctahedral clusters, underlining the importance of defect clustering in UO_{2+x} . Making use of the point defect model, an equation of state for non-stoichiometric oxides is established, which is then applied to describe the shock Hugoniot of UO_{2+x} . Furthermore, the oxidization and compression behavior of uranium monoxide, triuranium octoxide, uranium trioxide, and a series of defective UO_2 at zero Kelvin are investigated. The evolution of mechanical properties and electronic structures with an increase of the oxidation degree are analyzed, revealing the transition of the groundstate of uranium oxides from metallic to Mott insulator and then to charge-transfer insulator due to the interplay of strongly correlated effects of $5f$ orbitals and the shift of electrons from uranium to oxygen atoms.

PACS numbers: 61.72.J-, 62.50.-p, 71.15.Nc, 71.27.+a

Keywords: defects in solid, nonstoichiometric oxides, equation of state, lattice vibration, high-pressure physics

I. INTRODUCTION

Uranium oxides, especially uranium dioxide (UO_2), are interesting materials from a fundamental point of view, not only because of their complex electronic structure arisen from partially filled $5f$ electron shells and as materials of great technological importance in nuclear applications, but also because they are typical nonstoichiometric compounds. UO_2 manifests fluorite structure at all temperatures up to the melting point and pressures up to 40 GPa,^{1,2} as well as a wide range of off-stoichiometry.³⁻⁵ A comprehensive understanding of its thermodynamical, structural, and kinetic properties under extreme conditions is very important, especially for nuclear industry since UO_2 is the main fuel component for pressurized water reactors. Point defects are the key contents for these properties, particularly under irradiation as they play a major role in atomic diffusion. They also act as accommodation of the strong stoichiometry variations that exist in this material and provide incorporation sites for the fission products.

There are some theoretical studies on the properties of point defects⁶⁻¹⁵ and their incorporation with fission products¹⁶⁻²¹ in UO_2 at atomic-scale. Early literature used mainly empirical potentials,^{16,17} while recently the ones based on density functional theory (DFT) prevail. Since the standard local density approximation (LDA) or generalized gradient approximation (GGA) for the exchange-correlation functional fails to reproduce the fact that UO_2 is a Mott-Hubbard insulator with an energy gap split by the strongly correlated uranium $5f$ electrons,²²⁻²⁴ current *state of the art* approaches make use of DFT+ U formalism or the hybrid functional method to describe the electronic structure of UO_2 .^{2,24-26} With these methods, the formation energy of point defects in UO_2 at zero Kelvin were extensively studied,^{8-15,20,21} including both neutral and charged defects. The population of point defects at finite temperatures and partial oxygen pressures were also investigated based on these 0 K formation energies.

After these efforts, understanding of the electronic structure, magnetic ordering, atomic structural geometry, and energetics of perfect UO_2 and single point defects in it was advanced enormously. Nevertheless a fundamental experiment observation that oxygen defects predominate in the hyperstoichiometric regime still can not be reproduced, even at a qualitative level.^{6,7,15} Only one LSDA+ U calculation predicted the predominance of oxygen interstitial in this region.⁹ However, the agreement is quite marginal. On the other hand, if taking oxygen defect clustering into account, the predominance of oxygen defects in a form of cuboctahedral cluster can be easily established,^{27,28} indicating the complicated nature of this problem.

Furthermore, almost all of the previous investigations predicted a negative formation energy for single oxygen interstitial O_i , except one of the DFT+ U calculations with a GGA exchange-correlation functional that predicted a positive value of 0.1 eV.¹⁴ This is sharply in contrast to other DFT+ U and empirical results which usually are about $-1 \sim -3$ eV.^{9,10,15} It does not sound unreasonable considering that the hyperstoichiometric phase of UO_2 is unstable at 0 K.²⁹ However, it is worthwhile to note that a negative formation energy of O_i does not conflict with this observation too, since oxygen clusters have a lower energy^{9,27,28,30} and phase separation between the ordered phases of fluorite UO_2 and U_4O_9 ³¹⁻³³ could also lead to the same phase diagram. Nevertheless, a formation energy of O_i being apparently positive indicates a different oxidization mechanism, in which the lattice vibrations, or equivalently the phonons, should play a pivotal role at finite temperature and therefore alter the sign of the formation energy. This part of the contribution to the stability of defects in $\text{UO}_{2\pm x}$, however, was totally absent in almost all of the previous investigations. It now becomes imperative to assess the role played by this part of free energy on the energetics of defects.

In addition to reducing the free energy, lattice vibration at high temperature also leads to thermal expansion. The resultant dilation of the system volume inevitably changes the equilibrium 0 K formation energy. The influence of this effect on defect populations, as well as that due to possible residual stress arisen from irradiation damages, are unclear, which is possibly a partial consequence of the fact that the hydrostatic compression behavior and the equation of state (EOS) of solid $\text{UO}_{2\pm x}$ drew little attention in the past decades.³⁴ These mechanical properties now become important. It is crucial to know how the fuel components respond to shock waves generated at nearby explosions to assess the general safety of nuclear reactors and spent fuel storage facilities. Attempts to address these problems require a profound understanding of defects behavior at high-temperature high-pressure conditions, as well as a full EOS for non-stoichiometric fuel compounds.

In this paper, we evaluate the importance of lattice vibration and hydrostatic compression on the energetics and population of point defects in UO_2 with DFT+ U calculations. An equation of state model for off-stoichiometric $\text{UO}_{2\pm x}$ is then developed. It will benefit the understanding of other compounds since UO_2 is a typical non-stoichiometric oxide, and an EOS theory developed for it can be easily adapted for other alike materials. We also attempt to answer the question of whether oxygen clusters are definitely necessary or not in order to make oxygen defects the major component when contributions of phonon and thermal expansion have been taken into account. In addition, in order to demonstrate the overall trend of oxidation effects and highlight the crucial role played by $\text{UO}_{2\pm x}$, the energetics and electronic structures of uranium monoxide (UO), triuranium octoxide (U_3O_8), and uranium trioxide (UO_3) are investigated as well. The calculation methodology and the theoretical formalism are presented in the next section. The results and discussion are given in Sec. III, which is then followed by a summary of the main conclusions.

TABLE I. First-principles results for the energy curves of UO, $\text{UO}_{2\pm x}$, $\alpha\text{-U}_3\text{O}_8$, and $\delta\text{-UO}_3$, where x is the deviation from the stoichiometric composition of uranium dioxide and N is the total number of atoms in the simulation cell. D (in eV), r_0 (in Å), and B_0 (in GPa) are the cohesive energy per atom, the equilibrium lattice parameter of the effective cubic cell, and the zero pressure bulk modulus, respectively.

Label	x	N	Functional	D	r_0	B_0	Phase
UO	-1	8	GGA-PBE	7.446	4.875	187.58	NaCl (FM)
${}^u\text{C}4_1$	$-\frac{2}{17}$	49	LSDA+ U	8.045	5.513	198.83	CaF_2 (AFM)
$\text{C}4_{-1}$	$-\frac{1}{16}$	47	LSDA+ U	8.171	5.448	210.35	CaF_2 (AFM)
${}^u\text{C}8_1$	$-\frac{2}{33}$	97	LSDA+ U	8.135	5.481	212.39	CaF_2 (AFM)
$\text{C}8_{-1}$	$-\frac{1}{32}$	95	LSDA+ U	8.197	5.449	215.78	CaF_2 (AFM)
$\text{C}1$	0	12	LSDA+ U	8.219	5.452	215.55	CaF_2 (AFM)
$\text{C}8_1$	$\frac{1}{32}$	97	LSDA+ U	8.187	5.443	221.63	CaF_2 (AFM)
$\text{C}4_1$	$\frac{1}{16}$	49	LSDA+ U	8.145	5.439	202.14	CaF_2 (AFM)
${}^u\text{C}8_{-1}$	$\frac{2}{31}$	95	LSDA+ U	8.154	5.435	212.37	CaF_2 (AFM)
${}^u\text{C}4_{-1}$	$\frac{2}{15}$	47	LSDA+ U	8.085	5.410	200.38	CaF_2 (AFM)
$\text{COT-}o$	$\frac{5}{32}$	101	LSDA+ U	8.079	5.436	210.12	CaF_2 (AFM)
$\text{C}1_1$	$\frac{1}{4}$	13	LSDA+ U	7.937	5.402	246.63	CaF_2 (AFM)
$\alpha\text{-U}_3\text{O}_8$	$\frac{2}{3}$	11	GGA-PBE	7.594	5.537	165.81	$\text{Amm}2$ (FM)
$\delta\text{-UO}_3$	1	4	GGA-PBE	7.415	4.168	147.21	$\text{Pm}\bar{3}m$ (NM)

II. METHODOLOGY

A. Ground-state energy calculation

The energetics of UO, U_3O_8 , UO_3 , and a series of defective UO_2 in fluorite structures (to model off-stoichiometric $\text{UO}_{2\pm x}$) were studied through calculating the total energy curves with the plane-wave method using the density functional theory to treat the electronic energy as implemented in the VASP code.^{35,36} The electron-ion interactions were described by projector-augmented wave (PAW) pseudopotentials.^{37,38} The $2s^22p^4$ electrons in oxygen and $6s^26p^65f^36d^17s^2$ in uranium were treated in valence space. For UO_2 , the electronic exchange-correlation energy was computed by spin-polarized local density approximation with an effective on-site Coulomb repulsive interaction to split the partially filled $5f$ bands that localized on uranium atoms (LSDA+ U).³⁹⁻⁴¹ The LSDA+ U energy functional is given by

$$E_{\text{LSDA}+U} = E_{\text{LSDA}} + E_{\text{Hub}} - E_{\text{dc}}, \quad (1)$$

where E_{LSDA} is the LSDA contribution to the energy, E_{Hub} is the electron-electron interactions from the Hubbard term, and E_{dc} is the double-counting correction. The LSDA+ U approximation is thus a correction to the standard LSDA energy functional. E_{Hub} and E_{dc} depend on the occupation matrices of the correlated orbitals. We used the simplified rotationally invariant approximation for the Hubbard term E_{Hub} due to Dudarev *et al.*⁴¹ As regards the double counting correction, we used the fully localized limit, whose expression is

$$E_{\text{dc}} = \frac{U}{2} \hat{N}(\hat{N} - 1) - \frac{J}{2} \sum_{\sigma} \hat{N}^{\sigma}(\hat{N}^{\sigma} - 1). \quad (2)$$

Parameters of the Hubbard term were taken as $U = 4.5$ eV and $J = 0.51$ eV, which have been checked carefully for *fluorite* UO_2 .^{2,23,24,42} The possible metastable states introduced by strong correlation effects were removed via a quasiaannealing procedure,²¹ which has the capability of yielding the same results as an alternative but powerful approach of monitoring the occupation matrices.^{21,43} Previous investigation implied that the value of the Hubbard parameters depends on the local coordination environment,² and thus it should not be the same for different oxides. Since there are no appropriate values of U and J available for UO, U_3O_8 , and UO_3 , we used the pure GGA with the Perdew-Burke-Ernzerhof (PBE) exchange-correlation functional⁴⁴ instead of DFT+ U , which usually produces adequate energetics for uranium oxides even though the predicted electronic structure might be wrong.² The validity of such treatment is guaranteed by comparing the calculated lattice parameters with experimental data. The cutoff for kinetic energy of plane waves was set as high as 500 eV to converge the electronic energy within a few *meV* per atom.

Integrations over reciprocal space were performed in the irreducible Brillouin zone with about 8~36 non-equivalent k-points, depending on the system size.

In this work, we did not take spin-orbit coupling into account. Previous calculations on metallic α -U,^{7,45} perfect UO_2 ,² and U_3O_8 ⁴⁶ indicated that spin-orbit coupling has little effect on the structure and energy variation of uranium oxides, although it is well known that it is remarkable for magnetic properties. The only exception was reported by Yu *et al.*¹¹ Because inclusion of spin-orbit coupling in DFT+ U deteriorates the already notorious problem of metastable states and convergence, and they did not employ any special technique to tackle this problem, it is highly possible that the reported results are due to premature calculations that trapped in metastable states. This can be inferred from the jagged variation (which is quite unphysical) of the calculated lattice constant with U , as shown in Fig.3 of Ref.[11]. All of this indicates that their conclusion is still inconclusive. Based on these considerations, we neglected spin-orbit coupling in all of the following calculations.

The *supercell* method has been employed with periodic boundary conditions. The arrangement of the structures is listed in Table I, in which Cm_n denotes a defective UO_2 structure consisting of m fluorite cubic cells with n oxygen interstitials (or vacancies if n is negative).⁹ The superscript u indicates the defect is with respect to uranium. For example, configuration ${}^u C8_1$ has the same geometry as $C8_1$ but replacing the interstitial oxygen with a uranium atom, and ${}^u C8_{-1}$ or $C8_{-1}$ corresponds to removing one lattice atom (uranium and oxygen, respectively) from a structure with 8 fluorite cubic cells ($2 \times 2 \times 2$). Before calculating the energy, all structures were fully relaxed until residual Hellman-Feynman forces (stress) were less than 0.01 eV/Å.

Cohesive energies at different volumes are extracted from the total energies by subtracting the contribution of isolated spin-polarized atoms. They are then fitted to a Birch-Murnaghan equation of state,

$$E_c(V) = -D + \frac{9}{8}B_0V_0 \left[\left(\frac{V_0}{V} \right)^{\frac{2}{3}} - 1 \right]^2, \quad (3)$$

to facilitate post-analysis, where the equilibrium atomic volume V_0 can be determined from the effective lattice parameter as listed in Table I. With this equation, the pressure at 0 K can be expressed as

$$P_c(V) = \frac{3}{2}B_0 \left[\left(\frac{V_0}{V} \right)^{\frac{2}{3}} - 1 \right] \left(\frac{V_0}{V} \right)^{\frac{5}{3}}. \quad (4)$$

B. Formation Gibbs free energy

Phonon contribution to free energy and thermodynamic properties can be computed via lattice dynamics or molecular dynamics simulations. After getting the vibrational density of states $g(\omega)$, the thermal part of the Helmholtz free energy per atom in quasi-harmonic approximation reads

$$F_{ph}(V, T) = k_B T \int_0^\infty g(\omega) \ln [2 \sinh(\hbar\omega/2k_B T)] d\omega. \quad (5)$$

This method is accurate when anharmonic effect is insignificant. But the calculation is extremely demanding for *ab initio* simulations, especially for defective structures containing more than 90 atoms without any symmetry, as discussed here. Crude approximation includes computing the inter-atomic forces from empirical potentials⁴⁷ instead of by DFT calculations, while for off-stoichiometric compounds it is difficult to construct an accurate inter-atomic potential that maintains the charge neutrality of the cell generally.

For practical purposes, we resorted to the Debye model, which is less accurate but much easier for computation. More important is that it provides a convenient description of lattice dynamics with a qualitative picture (even quantitative sometimes), and this is enough for our discussion here. In the Debye model, Eq.(5) reduces to

$$F_{ph}(V, T) = 3k_B T \ln [1 - \exp(-\Theta_D/T)] - k_B T f(\Theta_D/T) + \frac{9}{8}k_B \Theta_D, \quad (6)$$

where k_B is the Boltzmann constant and f is the Debye function. The Debye temperature is approximated as^{48,49}

$$\Theta_D = \Theta_D^p \left[\frac{BM^p}{B^p M} \left(\frac{V}{V^p} \right)^{1/3} \right]^{1/2}. \quad (7)$$

Here the superscript p denotes the reference state (here the defect-free UO_2), B is the bulk modulus, V is the effective volume per atom, and M is the effective atomic weight. This approximation works well for a lot of materials,^{48,49}

and is a physically sound extrapolation for Θ_D of $\text{UO}_{2\pm x}$ from that of perfect UO_2 . The value of the latter, *i.e.* Θ_D^p , takes 383 K at ambient conditions according to recent x-ray diffraction analysis.^{50,51}

The Gibbs free energy for a specific defective structure i is then given by

$$G_i(P, T) = E_c(V) + F_{ph}(V, T) + PV. \quad (8)$$

For intrinsic point defects, the formation Gibbs free energy (FGE) of a Frenkel pair (FP) of species X is expressed as

$$G_{\text{X-FP}} = G_{X_v}^{N-1} + G_{X_i}^{N+1} - 2G^N, \quad (9)$$

and for the Schottky defect (S) as

$$G_S = G_{\text{U}_v}^{N-1} + 2G_{\text{O}_v}^{N-1} - 3\frac{N-1}{N}G^N. \quad (10)$$

If oxygen clusters are considered, we have to introduce isolated oxygen vacancy (O_v) to maintain the composition equation when in the closed regime where no particle exchange with the exterior occurs. For cuboctahedral clusters (COT), we thus should consider the O_v -COT complex and its FGE reads

$$G_{\text{COT}} = G_{\text{COT}}^{N+y} + yG_{\text{O}_v}^{N-1} - (y+1)G^N, \quad (11)$$

where y is the excess number of oxygen and takes 5 in the COT- o cluster.^{9,27} In these equations, N is the number of atoms in a defect-free cell (96 for a $2 \times 2 \times 2$ supercell) and G^N is the corresponding Gibbs free energy. $G_{X_v, X_i}^{N\pm 1}$ and G_{COT}^{N+y} are the Gibbs free energy of the cell containing the respective defect.

It is worthwhile to mention that the COT cluster was originally proposed by experimentalists to explain the measured neutron diffraction patterns of U_4O_9 ^{32,33} and U_3O_7 .^{52,53} Historically, it was denoted by M_6X_{36} (or M_6X_{37} if an additional anion occupies the center).^{32,54} However, it is a little misleading since the actual defect is composed of only 12 interstitials (forming the cuboctahedral geometry) and eight oxygen vacancies. There are two possible configurations for COT: with its center being occupied by another oxygen (COT- o) or being empty (COT- v). It was suggested that COT clusters should also present in UO_{2+x} .^{9,27,55} Its geometry, energetics, and structural stability have been discussed in Ref.[27].

III. RESULTS AND DISCUSSION

A. Properties at zero Kelvin

1. Uranium monoxide

In order to understand the general oxidation effects on compression behavior of uranium oxides, as well as to evaluate the significance of point defects on EOS of $\text{UO}_{2\pm x}$, we studied UO , the α phase of U_3O_8 , and the δ phase of UO_3 . UO is face-centered cubic with the sodium chloride-type structure. The experimental lattice parameter is $4.92 \pm 0.02 \text{ \AA}$.⁵⁶ However, there have been no claims of bulk UO having ever been synthesized, and reports of a UO surface phase on U metal for low exposures to oxygen⁵⁷ and UO thin films⁵⁶ could not be reproduced.⁵⁸ Since UO has never been prepared with great purity, it has been suggested that the observed thin films actually represent uranium oxynitrides and oxycarbides, which form in the presence of N_2 or C , and at low oxygen pressure.⁵⁹ The equilibrium lattice parameter and electronic structure of UO have been studied theoretically by density functional method,^{60,61} but no mechanical property and compression behavior were explored, which are important for the purpose of understanding the response of the materials being oxidized from metal to dioxide and then to trioxide.

Our calculated electronic density of states (DOS) is shown in the upper panel of Fig.1. For UO , the f -electron lingers between the localized and delocalized pictures. Here we assumed itinerant f electrons and in the ground state it is metallic, as can be seen from the nonzero DOS at the Fermi level. The O atom has two unoccupied p states, and in the monoxide, the p band can accommodate two electrons from the uranium atoms ($7s^2$) through charge transfer and hybridize with $6p^65f^36d^1$ weakly. The remaining valence electrons, including $6d$ and partially localized $5f$ electrons, start filling the conduction band, with the Fermi level pinned to the narrow f band. This agrees with earlier self-interaction-corrected local spin-density (SIC-LSD) approximation calculations.⁶¹ The energy curves shown in Fig.2 confirm that UO is in ferromagnetic (FM) ordering, with the anti-ferromagnetic (AFM) and non-magnetic (NM) configurations having an energy per cubic cell about 0.43 and 0.72 eV higher, respectively. A NM ordering state gives a shorter lattice parameter (4.84 \AA) and a higher bulk modulus (201 GPa), compared with early LDA results of 4.88 \AA and 198 GPa.⁶⁰ Meanwhile AFM and FM ordering have almost the same lattice parameter of 4.88 \AA , which is in good agreement with the experimental⁵⁶ value of 4.92 \AA and the SIC-LSD⁶¹ result of 4.94 \AA .

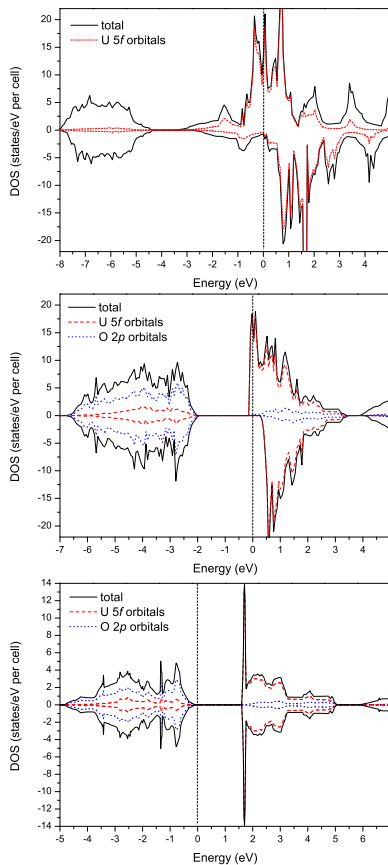


FIG. 1. (Color online) The total and partial electronic density of states that projected onto the U $5f$ and O $2p$ orbitals for UO (upper panel), α - U_3O_8 (middle panel), and δ - UO_3 (lower panel) at 0 GPa. Vertical dotted lines indicate the position of the Fermi levels.

TABLE II. Calculated lattice parameters (in \AA) and cell volume (in \AA^3) of α - U_3O_8 compared with other theoretical and experimental results.

Approach		a	b	c	Vol
PBE	FM, half-metallic	4.16	11.57	7.03	338.36
PBE	NM, metallic	4.16	11.77	6.87	336.38
GGA+ U ⁴⁶	FM, insulator	4.21	11.61	7.20	351.92
Expt. ⁶⁴	Insulator	4.15	11.95	6.72	333.26
Expt. ⁶³	Insulator	4.14	11.96	6.72	332.74

2. Triuranium octoxide and uranium trioxide

U_3O_8 is present as an olive green to black, odorless solid. In the presence of oxygen, uranium dioxide is oxidized to U_3O_8 , whereas UO_3 loses oxygen at temperatures above 773 K and is reduced to U_3O_8 .⁶² It is generally considered to be the more attractive form for disposal purposes of nuclear fuel because, under normal environmental conditions, U_3O_8 is one of the most kinetically and thermodynamically stable forms of uranium and also because it is the form of uranium found in nature. At low temperature U_3O_8 is in the α phase, a layered orthorhombic structure with space group $Amm2$,^{63,64} where the layers are bridged by oxygen atoms. Each layer contains uranium atoms which are in different coordination environments.

We studied the α - U_3O_8 phase by computing its atomic geometry, electronic structure, and energetics. Table II lists the calculated structure parameters by comparing with GGA+ U ⁴⁶ and experimental^{63,64} results. It can be seen that although pure GGA calculations with PBE functional fail to predict the correct insulator state, the optimized geometry is in good agreement with experimental measurements, except a slightly shorter b axis and a longer c axis

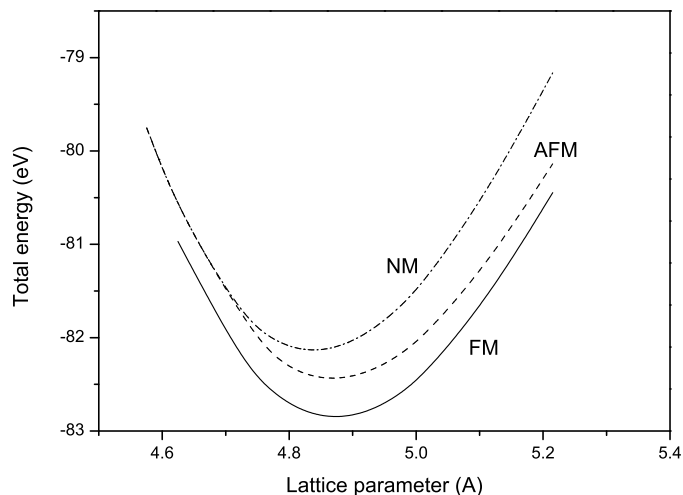


FIG. 2. Total energy variation of UO in different magnetic ordering states as a function of the cubic lattice parameter.

were obtained. Deviation of the predicted equilibrium volume from the measured ones is less than 2%. In contrast, GGA+ U predicts a much worse result, with the equilibrium volume about 6% larger.⁴⁶ This is quite similar to the embarrassing situation encountered by the GGA+ U approach in UO_2 , where a remarkable underestimation of the structural binding was also obtained.² Considering the acceptable performance of pure GGA on the energetics and EOS of UO_2 , we can expect that it will give reasonable results for the properties of U_3O_8 of interest here, even if a wrong half-metallic groundstate was predicted.

The electronic structure of non-magnetic $\alpha\text{-U}_3\text{O}_8$ shows that it is metallic with the Fermi level pinned at the bottom of the conduction band. The energy gap below it is about 2.2 eV. The FM ordering phase has an energy about 0.3 eV lower per conventional cell than the NM ordering one, and is half-metallic. This energy gain is from pushing the minor spin component of the $5f$ band away from the Fermi level. However, the remaining $5f$ electrons on uranium atoms occupy the major spin band and partially localize at the Fermi level (see the middle panel of Fig.1). If Hubbard on-site correction were applied, the narrow $5f$ band would be completely pushed away from the Fermi level and result in an insulator solution.

Local magnetic moment is a helpful indicator for the localization degree of $5f$ electrons. It is about $2\mu_B$ per uranium atom for UO and $1.93\mu_B$ for UO_2 ,² suggesting there are almost two $5f$ electrons being partially localized. The difference is that in UO the localized electrons are at the Fermi level in the conduction band, whereas in UO_2 the on-site Hubbard interaction splits the $5f$ band and leads to an energy gap (*i.e.*, being Mott insulator), thus the electrons are localized in the valence band. On the other hand, U_3O_8 is close to being a charge-transfer insulator, in which $5f$ electrons are absorbed by oxygen to fill the empty $2p$ orbitals. But this process is incomplete and the remaining partially localized $5f$ electrons in the conduction band pinned at the Fermi level contribute about $0.7\mu_B$ per uranium atom, and make U_3O_8 a half-metallic ferromagnet in GGA approximation. To open up the energy gap, the on-site Coulomb repulsion correction must be involved, and thus U_3O_8 is an intermediate phase between the Mott insulator and the charge transfer insulator, as shown by the GGA+ U calculation.⁴⁶ This picture is in accordance with nominal chemical valence counting: on average each uranium atom bonds with 0.67 more oxygen in U_3O_8 than in UO_2 , thus it loses about 1.3 more electrons in the former compound. Namely, most parts of the two localized $5f$ electrons has been transferred to oxygen and only a small portion (0.7 electrons) is left behind. This charge transfer naturally creates a sharp energy gap just below the Fermi level, resulting in an almost closed shell on the uranium cores. We therefore predict that UO_3 would be a pure charge-transfer insulator with the bare uranium ions in the closed-shell Rn configuration.

Calculations on the δ phase of UO_3 confirms this argument. $\delta\text{-UO}_3$ is a cubic phase in ReO_3 structure with a space group $Pm\bar{3}m$.⁶⁵ The lower panel in Fig.1 illustrates its calculated electronic DOS. It is a non-magnetic insulator. No any local magnetic moment on the uranium atoms can be observed. A distinct band gap of 1.6 eV can be clearly seen, which is due to the transfer of electrons to oxygen atoms, and leaves behind an empty atomic like $5f$ band. As a result, the Fermi level moves to the top of the valence band. This completes the electronic structure evolution of uranium oxides along the oxidation process, *i.e.*, from metal ($\alpha\text{-U}$ and UO, NM/FM) to Mott insulator (UO_2 , AFM), to intermediate insulator (U_3O_8 , FM), and then to pure charge transfer insulator (UO_3 , NM) with a gradual shifting of the $5f$ electrons from uranium to oxygen atoms (see Fig.1). The correlation effect among $5f$ orbitals also changes from one end to the other: in UO_2 it is the strongest, whereas in UO_3 we expect no strongly correlated effect to

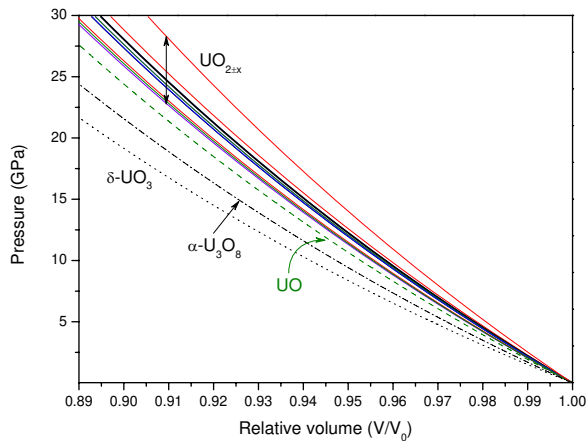


FIG. 3. (Color online) Compression curves of UO, α - U_3O_8 , and δ - UO_3 at zero Kelvin compared with that of $\text{UO}_{2\pm x}$; the latter spans a quite broad pressure range.

present at all. This can be verified by the correct prediction of the insulator groundstate of δ - UO_3 with the pure GGA approach, as well as the excellent agreement of the cubic lattice parameter between the calculated value of 4.168 Å and the experimental one of 4.165 Å.⁶⁵

3. Compressibility of $\text{UO}_{2\pm x}$

The ordered phase of U_4O_9 has a complicated structure consisting of $4 \times 4 \times 4$ fluorite-type subcells,³³ which is inaccessible for direct *ab initio* modeling because of the huge computational demands. We thus turn to the study of the $C1_1$ structure, as well as other defective $\text{UO}_{2\pm x}$ configurations as listed in Table I, and hope they can provide useful information on the general trend of oxidation effects on compression behavior. In $C1_1$ configuration there is one oxygen interstitial occupying the largest octahedral hole $(\frac{1}{2}, \frac{1}{2}, \frac{1}{2})$, and has the same chemical composition as U_4O_9 . But one should keep in mind that it is more a defective UO_2 rather than being U_4O_9 , and would overestimate the bulk modulus slightly because of its high symmetry.

The 0 K compression curves of defective $\text{UO}_{2\pm x}$ are shown in Fig.3, together with that of UO, α - U_3O_8 , and δ - UO_3 . The corresponding parameters for these curves are listed in Table I. It can be seen that although there might be some structure-dependence, a general trend is evident. With an increase of the oxidation degree from UO to UO_2 , the compound becomes harder and harder to compress, with the $C1_1$ configuration of $\text{UO}_{2\pm x}$ being the stiffest one. Further oxidization softens the material, and δ - UO_3 is the most compressible one. Please note that α - U_3O_8 and δ - UO_3 transform into other structures under compression at a pressure scale of several GPa. This makes the P - V lines kink at the transition points, and increase the compressibility further. A detailed analysis of these pressure-induced phase transitions are, however, beyond the scope of this paper.

The tendency due to oxidation also clearly manifests in Fig.4, where the correlation between cohesive energy, bulk modulus, and atomic volume is striking. Note that the values of α -U are taken from experiments,^{66,67} and others are the calculated results as listed in Table I. We can see that stoichiometric UO_2 has the largest cohesive energy per atom, thus being the most energetically stable phase, and reflects the fact that when heated to 1573 K U_3O_8 decomposes to UO_2 . As mentioned above, UO_2 , as well as $\text{UO}_{2\pm x}$, lies in the intermediate stage of the charge transfer process. Therefore it has the strongest covalent bonds that arise from hybridization between U $5f$ and O $2p$ orbitals, which then give rise to the smallest atomic volume, the deepest cohesive energy, and the highest bulk modulus, and therefore the least compressibility of $\text{UO}_{2\pm x}$ as shown in Fig.3. Further oxidization to U_3O_8 shifts the material quickly into ionic character, and the covalent bonds become weak. This leads to a huge volume expansion of more than 30%, and is dangerous for most nuclear application purposes.

It is worthwhile to point out that in Fig.3 the P - V lines of $\text{UO}_{2\pm x}$ span a wide range of pressure, and is comparable to the difference between stoichiometric UO_2 and other oxides. This underlines the importance of an accurate non-stoichiometric EOS, and it is inappropriate to *represent* it by any specific defective configuration, especially when the defect species change with temperature and pressure. Therefore a full EOS model is required for understanding the general thermophysical properties of off-stoichiometric compounds. That is, one has to study how the stoichiometry variation is accommodated in the material, what kind of microscopic entities are they in physics, and how these entities respond to different physical conditions. In the case of UO_2 , it is well known that point defects as well as

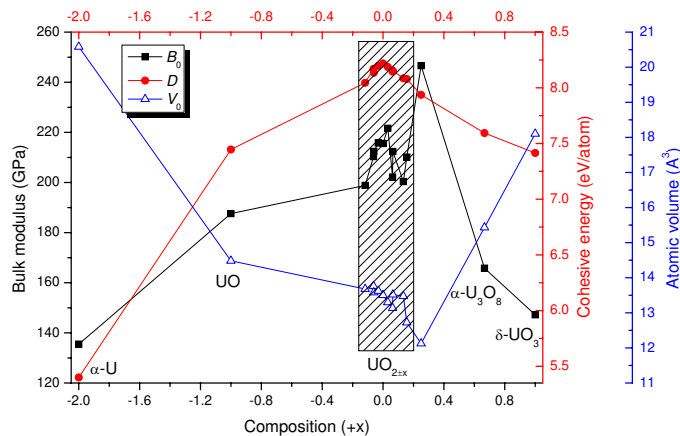


FIG. 4. (Color online) Variations of the cohesive energy per atom (D), the bulk modulus (B_0), and the atomic volume (V_0) as a function of composition deviation x at 0 GPa.

some oxygen clusters account for the stoichiometry variation while keeping the fluorite-type matrix almost unchanged. These features make the construction of the non-stoichiometric EOS much easier.

B. Finite pressures and temperatures

Almost all of the earlier defect population analyses were carried out with 0 K formation energies.^{6,7,9,15,27,28} It is widely assumed that the contribution from lattice vibrations is insignificant, but lacks detailed assessment. Also local residual stress and thermal expansion effects were completely neglected. The following discussion is devoted to this issue, and reveals that thermal vibrations have a limited but important influence on defect populations, whereas the pressure effect is much more striking in comparison.

It is worthwhile to note that since UO_2 is a semiconductor, the defects can be charged.^{10,15} These charged species might have several charge states.¹⁵ These facts and the slow convergence of a charged system in computation complicate the discussion (the energy converges linearly with respect to the inverse of the supercell size at the first order correction). Since our main purpose here is to investigate the phonon contribution and the compression effects on defects behavior, which should be similar for neutral and charged defects (we are reminded of the qualitative consistency of these two kinds of defects on 0 K formation energy^{10,15}), we thus focus our discussion here on neutral defects only. Extension of the analysis to charged defects is straightforward as long as the energetics of these species are known.

1. Variation of formation Gibbs free energy (FGE)

Variations of FGE as a function of temperature and pressure are shown in Fig.5 for intrinsic point defects (oxygen and uranium Frenkel pairs and Schottky defect, respectively) and in Fig.6 for the $\text{O}_v\text{-COT-}o$ complex, as defined in Eq.(11). It can be seen that phonon contribution reduces the FGE of the uranium Frenkel pair (FP), whereas it enhances that of the oxygen FP. As a result, its contribution to Schottky defect almost completely disappears due to cancellation of the opposite effect on uranium and oxygen defects. The maximum difference of the FGE between 0 and 1800 K is less than 0.62 eV for Frenkel pairs and 0.12 eV for Schottky defect, respectively. In other words, it counts only about 11% for oxygen FP, 4% for uranium FP, and 1% for Schottky defect.

The calculated FGE at 0 GPa and 0 K are consistent with that of Ref.[9]. But we have to point out that there is a typo in Ref.[9] where the formation energy of the uranium point interstitial (U-Int.) should be 5.642 eV instead of 8.194 eV. This change affects Table I and Table IV in Ref.[9]. Also, it reduces the energy of the uranium Frenkel pair (U-FP) in Table IV from 17.2 to 14.6 eV. However, this does not affect the defect population analysis since the concentration of uranium interstitial is too small to have any significant contribution to the stoichiometry of UO_2 .

On the other hand, lattice vibrations decrease the FGE of the $\text{COT-}o$ complex (see Fig.6). Increasing the temperature from 0 to 1800 K, the change in the FGE of the $\text{COT-}o$ complex is less than 0.72 eV, which is about 3% of the total formation energy. Compression depresses the phonon effects slightly. But totally, the thermal vibrational contribution to the FGE of point defects and the oxygen defect cluster is small.

In contrast, the compression effect is quite prominent. Within a pressure range of 30 GPa, which is easy to achieve

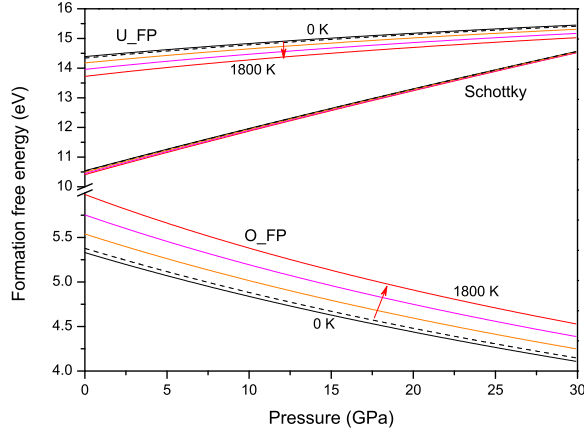


FIG. 5. (Color online) Variation of the formation Gibbs free energy of Frenkel pairs and Schottky defect in UO_2 under compression at different temperatures. Arrows indicate the direction of temperature increase with a step size of 600 K. Dashed lines correspond to 0 K results with zero point energy included.

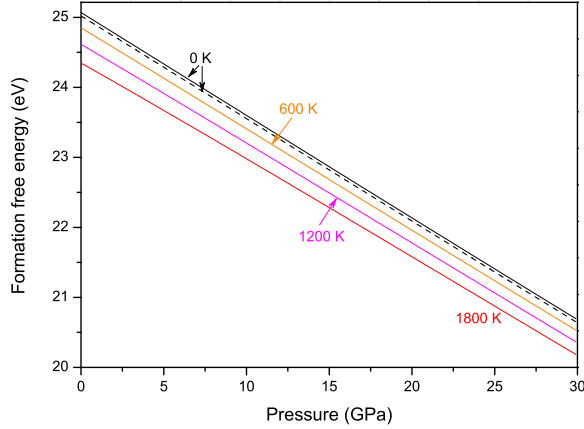


FIG. 6. (Color online) Formation Gibbs free energy of the COT-*o* complex as a function of temperature and pressure.

with diamond-anvil cell (DAC) devices or micro shock-wave loadings in nuclear materials driven by thermal spikes or collision cascade events arisen from fission reactions, the FGE increases 1.07, -1.23 , and 4.02 eV for uranium FP, oxygen FP, and Schottky defects, and amounts to 7%, -23% , and 38% of the zero pressure values, respectively. For the COT-*o* complex, the FGE change is -4.37 eV, about -17% of the 0 GPa value. Note that a pressure of 30 GPa corresponds to an energy scale of 2.4 eV per atom in UO_2 .

2. Defect populations

In addition to being a key content in the construction of a non-stoichiometric EOS,³⁴ the importance of analyzing defect populations, or equivalently the concentrations, also lies in the challenge of the elusive physics of UO_{2+x} . Although experiments have shown that COT-*o* clusters constitute the ordered phase of U_4O_9 on a fluorite matrix,^{31–33} it is still in debate whether or not such a cluster also appears in UO_{2+x} .^{4,5,27,28,55} Calculations using 0 K formation energy suggested that the existence of COT-*o* in UO_{2+x} is quite likely, but the observed ratio of oxygen interstitials occupying different sites cannot be accounted for quantitatively.^{27,28} This implies that we cannot exclude other possibilities. In this sense it is very important to figure out how the population of each possible defect changes with temperature and pressure. On the other hand, as mentioned above, one of the GGA+*U* calculations predicted a positive 0 K formation energy for point oxygen interstitial.¹⁴ If this reflects the true physical behavior, we can expect that phonon contribution at elevated temperatures should be as such that it makes oxygen defects the major component. These considerations underline the necessity to investigate the defect populations at different pressures and temperatures with phonon contributions having been taken into account.

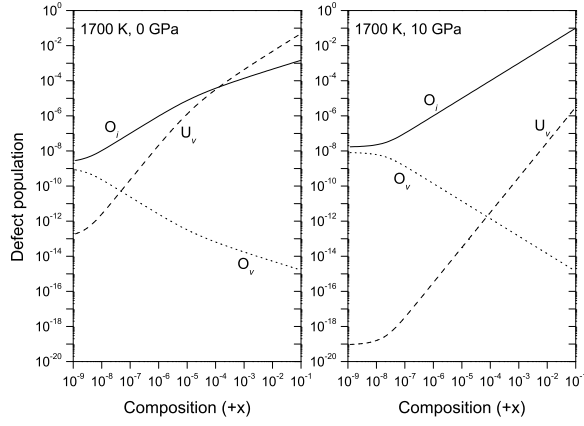


FIG. 7. Variation of concentrations of point defects at a temperature of 1700 K with x , the deviation from the stoichiometry of UO_2 in the hyper-stoichiometric regime: left is at a pressure of 0 GPa and right is under 10 GPa. Solid (dotted and dashed) line indicates the concentration in oxygen interstitial (oxygen vacancy and uranium vacancy). The concentration of uranium interstitial is negligible.

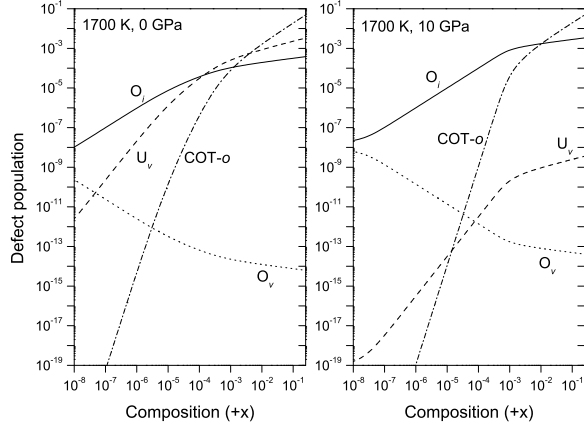


FIG. 8. The influence of oxygen cluster COT- o on defect concentrations at 0 and 10 GPa, respectively. The dash-dotted line indicates the concentration of COT- o cluster; others are the same as in Fig.7.

Using the point defect model (PDM) developed by Lidiard and Matzke,^{9,27,68,69} defect populations around the dilute limit can be computed. The key point is that here the FGE instead of the 0 K formation energies are employed. In the following we mainly discuss the hyperstoichiometric ($x > 0$) regime because in the other side of $x < 0$, it is always oxygen vacancy (O_v) that predominates. Although both pressure and temperature enhance the concentration of point oxygen interstitial (O_i) and uranium interstitial (U_i) slightly, they are still at least two orders smaller than that of O_v and can be neglected safely.

Figure 7 illustrates the defect populations as a function of composition at 1700 K under pressures of 0 and 10 GPa, respectively. By comparing with Fig.11 in Ref.[9] where only 0 K and 0 GPa formation energies were used in the PDM analysis, we find a slight decrease of the concentration of O_i and an increase of the uranium vacancy (U_v), and the latter becomes the major component when $x > 10^{-3}$. Both lattice vibrations and thermal expansion contribute to this change. From Fig.5 we learn that phonon favors uranium defects. Thermal expansion also prefers uranium FP and Schottky defect because at an elevated temperature thermal expansion leads to a larger volume that corresponds to a negative cold pressure, which reduces the formation energy of uranium FP and Schottky but lifts that of oxygen FP. This result is strongly against the experimental observation that oxygen defects are predominant in UO_2 at any temperature and stoichiometry.^{4,5,55,69} Increasing pressure can depress the uranium vacancy, as shown in the right panel of Fig.7. This is easy to understand by inspecting the variation of FGE with pressure as shown in Fig.5. Nevertheless, this compression effect is not enough to explain the observed predominance of oxygen defects because the possible residual stress within the fuel is usually less than 1 GPa, and at such a pressure scale the uranium vacancy is still comparable to oxygen defects.

It thus becomes interesting to investigate whether phonon and compression effects can alter the behavior of the

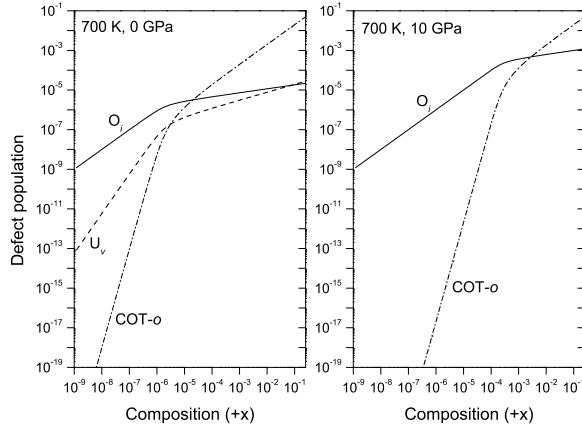
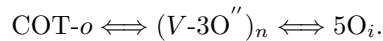


FIG. 9. The same as in Fig.8 but now with a temperature of 700 K.

COT-*o* cluster greatly or not. Earlier studies showed that when only 0K formation energies were used, the COT-*o* cluster is dominant at low temperature and high composition region.^{27,28} Figure 8 plots the variation of defect populations at 1700K with COT-*o* included. Note here that we didnot consider the internal degeneracy of this cluster,²⁷ since physically no two clusters can occupy the same lattice site simultaneously if we ignore quantum effects and treat oxygen as a classical particle. We can see that, as in the previous case, phonon contribution enhances uranium vacancy, which is very clear if comparing with Fig.3 of Ref.[27]. The earlier conclusion that COT-*o* is predominant is still preserved when $x > 10^{-2}$. At a pressure of 10 GPa, uranium vacancy is drastically suppressed, leaving only single oxygen interstitial and COT-*o* in competition (the right panel of Fig.8). Lowering the temperature to 700K further suppresses uranium vacancy and oxygen interstitial, as Fig.9 shows, meanwhile COT-*o* gets some promotion. Increasing the pressure to 10 GPa then sweeps all other defects away and leaves only O_i and COT-*o* clusters, with a slight depression of the latter and an enhancement of the former.

It is evident that lattice vibrations and hydrostatic compression change the competition among defects greatly, and the conclusions obtained with 0 K and 0 GPa formation energies need be revised: when considering only point defects, the earlier predicted predominance of O_i doesnot hold anymore with the full FGE, and U_v becomes the dominant defect when $x > 10^{-3}$. That is to say, at the full level of the theory the experimental fact cannot be reproduced if only neutral point defects are considered. On the other hand, when the COT-*o* cluster is taken into account, the predominance of this oxygen cluster can be easily established both at the full FGE level and at the 0K and 0 GPa formation energy level. The calculated results clearly demonstrate that hydrostatic pressure has a strong influence on defect populations, and oxygen clusters are definitely necessary in order to suppress the concentration of uranium vacancy to match the experimental observation qualitatively.

Considering the low temperature phase diagram²⁹ of UO_{2+x} and the negative formation free energy of O_i and COT-*o*, it becomes clear that the possibility of phase separation between UO_2 and U_4O_9 must be considered seriously if one wants to understand the underlying physics correctly. Because U_4O_9 can be viewed as an ordered phase of COT-*o* clusters on a fluorite matrix,^{32,33} this phase separation is in fact a process of formation and segregation of oxygen clusters. Thus at the intermediate composition and elevated temperature range where UO_{2+x} is stable, the dynamics of decomposition/formation of COT-*o* is crucial, as well as other competitive clusters such as $(V-3O'')_2$.^{12,21,28,30} It is worthwhile to highlight the connection between $V-3O''$ based clusters^{12,28,30} and cuboctahedral clusters^{27,32,33,55} (mainly COT-*o*). Although the latter is more stable at low temperature,^{27,28} it was predicted that with increasing temperature COT-*o* will gradually dissociate into a set of single point defects.²⁷ The intermediate state of this process is of great importance for understanding the kinetic behavior. The relatively low energy of $(V-3O'')_n$ makes it a promising candidate of this transition state.²¹ This is possible because the COT cluster in fact can be viewed as a complex formed by eight tightly connected $V-3O'$ clusters (a distorted version of $V-3O''$). Then partial dissociation of COT clusters will likely go through a configuration of $V-3O''/O'$ kinetically to lower the energy barrier; that is,



3. Non-stoichiometric equation of state and shock Hugoniot

Off-stoichiometry is widely observed in materials of many categories, for example, in ionic compounds (*e.g.*, oxides, nitrides, and carbides), alloys and intermetallic compounds, doped semiconductors, and high-temperature superconductors, and so on. In these materials, the underlying structure of the matrix is usually unchanged or just slightly distorted, but the electronic and magnetic properties can be controlled and tuned for application purposes. The maximal stoichiometry deviation indicates the capability of the matrix structure to tolerate distortions caused by doped elements or defects. The mechanical properties usually are determined by the matrix, but are also varied with respect to different chemical compositions.

The thermodynamic behavior of these materials across a wide range of temperature and pressure are of interest not only for fundamental physics and material science but also for engineering applications, in which EOS is one of the most important contents. There is an elegant theory developed on Ising models of lattice gases, namely, the cluster variation method (CVM),⁷⁰ which describes the phase diagram and EOS of binary and pseudo-binary alloys very well.^{48,71–74} To generalize this method beyond the ternary system is difficult. For ionic compounds, however, the stoichiometry usually is accommodated via defects, and is a multi-component system with the number of species greater than four. Furthermore, not all of these defects sit on the lattice site of the matrix, which complicates the construction of the theory, and slows down the convergence even if a CVM-like theory could be constructed.⁹ From this point of view, a different route should be attempted for a practical *ab initio* EOS model (*i.e.*, without any empirical parameters) of non-stoichiometric compounds.

Having known the defect concentrations, we can express the total Gibbs free energy G of a non-stoichiometric material at pressure P and temperature T as a function of the defect concentrations n_i that accommodate the stoichiometry deviation. Around the vicinity of the dilute limit, Taylor expansion of G with respect to n_i reads⁷⁵

$$G = G^p + \sum_i A_i n_i + \frac{1}{2} \sum_{i,j} B_{ij} n_i n_j + \dots, \quad (12)$$

where G^p is the Gibbs free energy of the matrix, A_i is the contribution of single defects, and B_{ij} is the interaction strength between defects, and so on. At the first order approximation we can express the non-stoichiometric Gibbs free energy by making use of specific defective structures as reference; that is,

$$G \approx G^p + \sum_i \frac{\Delta G_i}{n_i^{\text{ref}}} n_i. \quad (13)$$

Here the superscript “ref” indicates the defective reference system, n_i is the concentration of defect type i , and the Gibbs free energy difference is $\Delta G_i = G_i^{\text{ref}} - G^p$. Obviously this linear approximation assumes that the interaction term between defects B_{ij} is insignificant, which is only true at the dilute limit. However, making use of reference states extends the applicability of this approximation greatly. It is evident from Eq.(13) that G is close to being exact when $n_i = n_i^{\text{ref}}$. Nevertheless, within this linear approximation, the solubility of defects and spinodal decomposition of the system cannot be correctly described, where the nonlinear terms in Eq.(12) are essential.

Within this framework, the system volume becomes

$$V = V^p + \sum_i \frac{V_i^{\text{ref}} - V^p}{n_i^{\text{ref}}} n_i, \quad (14)$$

and this gives the equation of state for a non-stoichiometric material. Defect concentrations n_i at thermodynamic equilibrium conditions are determined with the composition equation using the point defect model as discussed above.

Hugoniot is a set of locus of thermodynamic states that describe the response of a material to shock wave loadings. It is governed by the law of energy conservation across the discontinuous zone generated by shock waves, *i.e.*,

$$E - E_0 = \frac{1}{2} (P + P_0) (V_0 - V), \quad (15)$$

and serves as an important content of high-pressure high-temperature EOS. For theoretical analysis, it is convenient to reformulate Eq.(15) as⁷²

$$G - G_0 = \frac{1}{2} (P - P_0) \left[\left(\frac{\partial G}{\partial P} \right)_{T, n_i} + \left(\frac{\partial G_0}{\partial P} \right)_{T, n_i} \right] + T \left(\frac{\partial G}{\partial T} \right)_{P, n_i} - T_0 \left(\frac{\partial G_0}{\partial T} \right)_{P, n_i}, \quad (16)$$

where G_0 is the system Gibbs free energy at an initial condition of pressure P_0 and temperature T_0 .

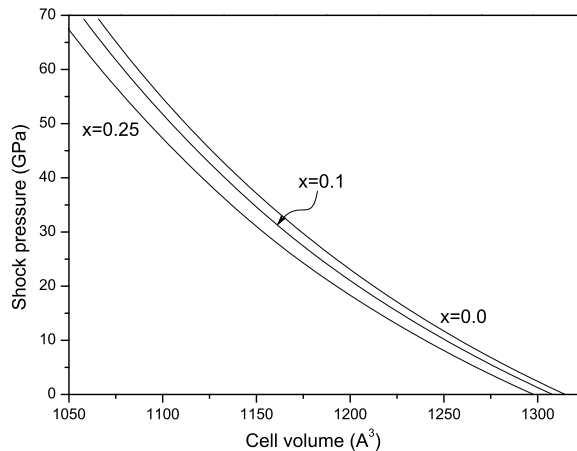


FIG. 10. Hugoniot of UO_{2+x} shocked from an initial state of 500 K and 0 GPa.

Taking the largest defective configurations as the reference structures (*i.e.*, *C8* and *COT-o* configurations as listed in Table I that are based on a $2 \times 2 \times 2$ supercell of fluorite cubes), the shock Hugoniot of UO_{2+x} up to 70 GPa were calculated and shown in Fig.10 with $x = 0, 0.1$, and 0.25 , respectively. Note that since here all defects are defined on a fluorite cubic cell of UO_2 , the Gibbs free energy G must be given with respect to the same cell. The initial condition of shock is at 0 GPa and 500 K. The highest shock temperature is less than 1200 K, reflecting the high bulk modulus of the material and thus a weak energy accumulation of shock waves. Although the cubic fluorite phase of UO_2 transforms into orthorhombic *Pnma* at room temperature beyond 42 GPa,^{1,2} the transition is rather sluggish and the fluorite phase persists up to 70 GPa.¹ This suggests the selected range of pressure in Fig.10 is appropriate. Beyond that pressure, we must reanalyze the geometry of defects and their occupation dynamics because the matrix has already been changed due to phase transition.

From Fig.10 we can see that the Hugoniot of UO_{2+x} is very similar to stoichiometric UO_2 , with the whole curve shifting to the left and reducing the cell volume correspondingly with an increase of x . This is reasonable because from the above analysis we learned that within this pressure and temperature range the *COT-o* cluster is always predominant, and the defective structure with this cluster has a very similar 0 K energy curve as that of UO_2 (see Table I). However, this is not always the case for non-stoichiometric compounds. Along the shock wave loading path, pressure and temperature change from point to point because of energy accumulations. If species of the major defect component were changed due to this kind of thermodynamic condition variation, the atomic scale behavior of defects would then manifest itself on the Hugoniot curve. In that case the non-stoichiometric EOS would be a useful tool to study this phenomenon theoretically and thoroughly.

IV. CONCLUSION

We have presented calculations, using the $\text{LSDA}+U$ exchange-correlation functional, of the high-temperature high-pressure properties of point defects in $\text{UO}_{2\pm x}$. The phonon contributions were taken into account via the Debye model. The results showed that lattice vibrations enhance the population of uranium vacancy slightly, whereas hydrostatic compression changes the energetics of all defects and then their populations greatly. At ambient pressure, however, inclusion of phonon free energy and thermal expansion effect fails to reproduce the experimental observation that oxygen defects should be predominant at the $x > 0$ regime, suggesting that the inclusion of defect clusters such as *COT-o* is necessary. Furthermore, both lattice vibrations and compression favor the *COT-o* cluster, and its predominance in the hyper-stoichiometric regime gets reinforced as compared with the results obtained with 0 K formation energies.

In order to understand the overall trend of oxidation effects, the 0 K electronic structures and equations of state of UO , $\text{UO}_{2\pm x}$, $\alpha\text{-U}_3\text{O}_8$, and $\delta\text{-UO}_3$ were investigated thoroughly, revealing the transition of the groundstate of uranium oxides from being metallic to Mott insulator and then to charge-transfer insulator across the full oxidation degree. Variations of cohesive energy, atomic volume, and stiffness of the oxides due to evolution of the chemical bonds from being metallic to covalent and then to ionic characteristics were well demonstrated. The necessity to develop an EOS model for off-stoichiometric compounds was also highlighted by comparing the compression curves of defective $\text{UO}_{2\pm x}$ with that of other uranium oxides. With the knowledge of defect populations within a wide range of pressure and temperature, a specific equation of state for non-stoichiometric compounds was constructed. The shock Hugoniot of

UO_{2+x} were then studied to illustrate the performance of this model.

ACKNOWLEDGMENTS

Support from the Fund of National Key Laboratory of Shock Wave and Detonation Physics of China (under Grant No. 9140C6703031004) is acknowledged.

-
- ¹ M. Idiri, T. Le Bihan, S. Heathman, and J. Rebizant, Phys. Rev. B **70**, 014113 (2004).
² H. Y. Geng, Y. Chen, Y. Kaneta, and M. Kinoshita, Phys. Rev. B **75**, 054111 (2007).
³ C. R. A. Catlow, in *Nonstoichiometric Oxides*, edited by O. T. Sørensen (Academic, New York, 1981).
⁴ B. T. M. Willis, Proc. Br. Ceram. Soc. **1**, 9 (1964).
⁵ B. T. M. Willis, Acta Crystallogr., Sect. A: Cryst. Phys., Diffr., Theor. Gen. Crystallogr. **A34**, 88 (1978).
⁶ J. P. Crocombette, F. Jollet, T. N. Le, and T. Petit, Phys. Rev. B **64**, 104107 (2001).
⁷ M. Freyss, T. Petit, and J. P. Crocombette, J. Nucl. Mater. **347**, 44 (2005).
⁸ M. Iwasawa, Y. Chen, Y. Kaneta, T. Ohnuma, H. Y. Geng, and M. Kinoshita, Mater. Trans. **47**, 2651 (2006).
⁹ H. Y. Geng, Y. Chen, Y. Kaneta, M. Iwasawa, T. Ohnuma, and M. Kinoshita, Phys. Rev. B **77**, 104120 (2008).
¹⁰ P. Nerikar, T. Watanabe, J. S. Tulenko, S. R. Phillpot, and S. B. Sinnott, J. Nucl. Mater. **384**, 61 (2009).
¹¹ J. Yu, R. Devanathan, and W. J. Weber, J. Phys.: Condens. Matter **21**, 435401 (2009).
¹² D. A. Andersson, T. Watanabe, C. Deo, and B. P. Uberuaga, Phys. Rev. B **80**, 060101(R) (2009).
¹³ F. Gupta, A. Pasturel, and G. Brillant, Phys. Rev. B **81**, 014110 (2010).
¹⁴ B. Dorado, G. Jomard, M. Freyss, and M. Bertolus, Phys. Rev. B **82**, 035114 (2010).
¹⁵ J. P. Crocombette, D. Torumba, and A. Chartier, Phys. Rev. B **83**, 184107 (2011).
¹⁶ C. R. A. Catlow, Proc. R. Soc. London, Ser. A **353**, 533 (1977).
¹⁷ R. W. Grimes and C. R. A. Catlow, Philos. Trans. R. Soc. London, Ser. A **335**, 609 (1991).
¹⁸ J. P. Crocombette, J. Nucl. Mater. **305**, 29 (2002).
¹⁹ M. Freyss, N. Vergnet, and T. Petit, J. Nucl. Mater. **352**, 144 (2006).
²⁰ P. V. Nerikar, X. Y. Liu, B. P. Uberuaga, C. R. Stanek, S. R. Phillpot, and S. B. Sinnott, J. Phys.: Condens. Matter **21**, 435602 (2009).
²¹ H. Y. Geng, Y. Chen, Y. Kaneta, M. Kinoshita, and Q. Wu, Phys. Rev. B **82**, 094106 (2010).
²² T. Petit, B. Morel, C. Lemaignan, A. Pasturel, and B. Bigot, Philos. Mag. B **73**, 893 (1996).
²³ S. L. Dudarev, D. N. Manh, and A. P. Sutton, Philos. Mag. B **75**, 613 (1997).
²⁴ S. L. Dudarev, G. A. Botton, S. Y. Savrasov, Z. Szotek, W. M. Temmerman, and A. P. Sutton, Phys. Status Solidi A **166**, 429 (1998).
²⁵ B. Dorado, B. Amadon, M. Freyss, and M. Bertolus, Phys. Rev. B **79**, 235125 (2009).
²⁶ K. N. Kudin, G. E. Scuseria, and R. L. Martin, Phys. Rev. Lett. **89**, 266402 (2002); I. D. Prodan, G. E. Scuseria, and R. L. Martin, Phys. Rev. B **73**, 045104 (2006); *ibid* **76**, 033101 (2007).
²⁷ H. Y. Geng, Y. Chen, Y. Kaneta, and M. Kinoshita, Phys. Rev. B **77**, 180101(R) (2008).
²⁸ H. Y. Geng, Y. Chen, Y. Kaneta, and M. Kinoshita, Appl. Phys. Lett. **93**, 201903 (2008).
²⁹ J. D. Higgs, W. T. Thompson, B. J. Lewis, and S. C. Vogel, J. Nucl. Mater. **366**, 297 (2007).
³⁰ D. A. Andersson, J. Lezama, B. P. Uberuaga, C. Deo, and S. D. Conradson, Phys. Rev. B **79**, 024110 (2009).
³¹ J. Hering and P. Perio, Bull. Soc. Chim. Fr. **19**, 351 (1952).
³² D. J. M. Bevan, I. E. Grey, and B. T. M. Willis, J. Solid State Chem. **61**, 1 (1986).
³³ R. I. Cooper and B. T. M. Willis, Acta Crystallogr., Sect. A: Found. Crystallogr. **A60**, 322 (2004).
³⁴ E. Yakub, C. Ronchi, and I. Iosilevski, J. Phys.: Condens. Matter **18**, 1227 (2006).
³⁵ G. Kresse and J. Furthmüller, Comput. Mater. Sci. **6**, 15 (1996).
³⁶ G. Kresse and J. Furthmüller, Phys. Rev. B **54**, 11169 (1996).
³⁷ P. E. Blöchl, Phys. Rev. B **50**, 17953 (1994).
³⁸ G. Kresse and D. Joubert, Phys. Rev. B **59**, 1758 (1999).
³⁹ V. I. Anisimov, J. Zaanen, and O. K. Andersen, Phys. Rev. B **44**, 943 (1991).
⁴⁰ A. I. Liechtenstein, V. I. Anisimov, and J. Zaanen, Phys. Rev. B **52**, R5467 (1995).
⁴¹ S. L. Dudarev, G. A. Botton, S. Y. Savrasov, C. J. Humphreys, and A. P. Sutton, Phys. Rev. B **57**, 1505 (1998).
⁴² S. L. Dudarev, M. R. Castell, G. A. Botton, S. Y. Savrasov, C. Muggelberg, G. A. D. Briggs, A. P. Sutton, and D. T. Goddard, Micron **31**, 363 (2000).
⁴³ B. Dorado, B. Amadon, G. Jomard, M. Freyss, and M. Bertolus, Phys. Rev. B **84**, 096101 (2011).
⁴⁴ J. P. Perdew, K. Burke, and M. Ernzerhof, Phys. Rev. Lett. **77**, 3865 (1996).
⁴⁵ P. Söderlind, Phys. Rev. B **66**, 085113 (2002).
⁴⁶ Y. Yun, J. Ruzs, M. T. Suzuki, and P. M. Oppeneer, Phys. Rev. B **83**, 075109 (2011).
⁴⁷ T. Watanabe, S. G. Srivilliputhur, P. K. Schelling, J. S. Tulenko, S. B. Sinnott, and S. R. Phillpot, J. Am. Ceram. Soc. **92**, 850 (2009).

- ⁴⁸ H. Y. Geng, M. H. F. Sluiter, and N. X. Chen, Phys. Rev. B **72**, 014204 (2005).
- ⁴⁹ V. L. Moruzzi, J. F. Janak, and K. Schwarz, Phys. Rev. B **37**, 790 (1988).
- ⁵⁰ H. Serizawa, Y. Arai, M. Takano, and Y. Suzuki, J. Alloys Compd. **282**, 17 (1999).
- ⁵¹ H. Serizawa, Y. Arai, and Y. Suzuki, J. Nucl. Mater. **280**, 99 (2000).
- ⁵² F. Garrido, R. M. Ibberson, L. Nowicki, and B. T. M. Willis, J. Nucl. Mater. **322**, 87 (2003).
- ⁵³ L. Nowicki, F. Garrido, A. Turos, and L. Thome, J. Phys. Chem. Solids **61**, 1789 (2000).
- ⁵⁴ D. J. M. Bevan and S. E. Lawton, Acta Crystallogr., Sect. B: Struct. Sci. **B42**, 55 (1986).
- ⁵⁵ A. D. Murray and B. T. M. Willis, J. Solid State Chem. **84**, 52 (1990).
- ⁵⁶ D. J. Lam, J. B. Darby, and M. B. Newitt, in *The Actinides, Electronic Structure and Related Properties*, edited by A. J. Freeman and J. B. Darby (Academic, New York, 1974), Vol. 11, p. 119.
- ⁵⁷ W. P. Ellis, Surf. Sci. **61**, 37 (1976).
- ⁵⁸ K. Winer, C. A. Colmenares, R. L. Smith, and F. Wooten, Surf. Sci. **177**, 484 (1986).
- ⁵⁹ M. Eckle and T. Gouder, J. Alloys Compd. **374**, 261 (2004).
- ⁶⁰ M. S. S. Brooks, J. Phys. F: Met. Phys. **14**, 639 (1984).
- ⁶¹ L. Petit, A. Svane, Z. Szotek, W. M. Temmerman, and G. M. Stocks, Phys. Rev. B **81**, 045108 (2010).
- ⁶² T. Fujino, H. Tagawa, and T. Adachi, J. Nucl. Mater. **97**, 93 (1981).
- ⁶³ B. O. Loopstra, J. Appl. Crystallogr. **3**, 94 (1970).
- ⁶⁴ C. G. S. Pillai, A. K. Dua, and P. Raj, J. Nucl. Mater. **288**, 87 (2001).
- ⁶⁵ M. T. Weller, P. G. Dickens, and D. J. Penny, Polyhedron, **7**, 243 (1988).
- ⁶⁶ C. S. Barrett, M. H. Mueller, and R. L. Hittermann, Phys. Rev. B **129**, 625 (1963).
- ⁶⁷ C. S. Yoo, H. Cynn, and P. Söderlind, Phys. Rev. B **57**, 10359 (1998).
- ⁶⁸ A. B. Lidiard, J. Nucl. Mater. **19**, 106 (1966).
- ⁶⁹ H. J. Matzke, J. Chem. Soc., Faraday Trans. 2 **83**, 1121 (1987).
- ⁷⁰ R. Kikuchi, Phys. Rev. **81**, 988 (1951).
- ⁷¹ J. W. D. Connolly and A. R. Williams, Phys. Rev. B **27**, 5169 (1983).
- ⁷² H. Y. Geng, N. X. Chen, and M. H. F. Sluiter, Phys. Rev. B **71**, 012105 (2005).
- ⁷³ M. Sluiter, D. de Fontaine, X. Q. Guo, R. Podloucky, and A. J. Freeman, Phys. Rev. B **42**, 10460 (1990).
- ⁷⁴ M. H. F. Sluiter, Y. Watanabe, D. de Fontaine, and Y. Kawazoe, Phys. Rev. B **53**, 6137 (1996).
- ⁷⁵ The configurational entropy contributed by independent point defects is proportional to $-k_B \sum_i N_i [n_i \ln n_i + (1 - n_i) \ln(1 - n_i)]$, where N_i is the number of available sites for defects. This term, however, is irrelevant when discussion of EOS is made for the closed regime only.